Georgia Institute of Technology – Aerospace Engineering, AE8900

A Method to Characterize Parachute System Instability Modes

Michael Bernatovich
Dr. Ian Clark
5/6/2013

A Method to Characterize Parachute System Instability Modes

Michael A. Bernatovich[1] and Dr. Ian Clark[2]
Georgia Institute of Technology, Atlanta, Georgia, 30332

A simplified, yet robust, parachute system stability analysis is performed using a 5-DOF (altitude, pitch, & yaw) descent trajectory simulation. Several trade studies are performed to determine what types of initial conditions and wind perturbations can result in pitching (i.e. planar) or coning instability modes. Building on these results, several vehicle design sensitivities are performed to roughly describe the trend in stability with canopy trailing distance, canopy diameter, & payload mass. As a complement to these sensitivities and trade studies, an early Mars EDL research drop test is analyzed as a case study. During this drop test, the system experienced uncharacteristically large pitch oscillations primarily driven by canopy vortex shedding. Data from this drop test will be used to determine the trajectory & vehicle design space within which this behavior could be expected.

Acronyms

AGL	Above Ground Level
CG	Center of Gravity
CP	Center of Pressure
MSL	Mars Science Laboratory
RSS	Root Sum Square

Symbols & Nomenclature

U, V, W	*Velocity components*
X, Y, Z	*Aerodynamic force components*
ρ	*Density*
D_o	*Canopy reference diameter*
m_p	*Payload mass*
m_c	*Canopy mass*
m_{app}	*Apparent mass*
m_{sys}	*System mass (payload & canopy)*
m_{tot}	*Total mass (system & apparent)*
g	*Gravity*
ψ	*Euler, rotation about vehicle Z_1 axis*
θ	*Euler, rotation about vehicle Y_2 axis*
φ	*Euler, rotation about vehicle X_3 axis*
P, Q	*System angular rates*
M, N	*Aerodynamic moment components*
L_P, L_C	*Distance to CG from payload & canopy CP*
I_{tot}	*Total moment of inertia*

[1] Graduate Student, Georgia Tech School of Aerospace Engineering, 2101 NASA Parkway, Mailcode: DM42, Houston, TX 77058.
[2] Visiting Professor, Georgia Tech School of Aerospace Engineering

I. Introduction

PARACHUTE system stability has proven to be one of the most difficult aspects of modeling parachutes due to the different stability modes to distinguish as well as the inherent bounded random nature of parachutes. Over the years, various approaches to modeling and characterizing this behavior have been proposed, modified, and practiced. While many of these approaches are useful, basic equations of motion are used to observe the initial conditions and disturbances that may result in certain instability modes for a specific system. The equations of motion and analysis approach for most of the present analysis build on that from a journal article written by Frank White & Dean Wolf, "A Theory of Three-Dimensional Parachute Dynamic Stability" [1]. White's paper used a non-dimensional approach to determine how the system will react to certain types of disturbances. This paper compliments their work by using the dimensional form of the same base equations of motion to characterize pure pitch & coning instability due to initial condition variations and range of vehicle design characteristics. Additionally, it addresses the influence that wind gusts can have on these different instability modes.

In addition to the aforementioned parachute instability mode analysis, a case study from a Mars technology drop test is explored. In this high-altitude, subsonic drop test, a Ringsail parachute system experienced uncharacteristically large, pendulum-like oscillations about the center of gravity during the upper altitude portion of descent. During post-flight reconstruction & analysis, the oscillatory behavior was identified as a "result of a resonance between the natural frequency of the system and the [canopy] vortex shedding frequency". This case study builds on this theory by attempting to define the trajectory & vehicle design spaces within which this behavior can be expected. Since this anomaly cannot be captured using simplified equations of motion, a parametric sweep of various trade-space factors is used.

II. Analysis Setup

A. Equations of Motion

In large part adopted from the White & Wolf article, the following system of equations make the following set of assumptions [1]:

- The system consists of a symmetric parachute rigidly connected to a neutral payload.
- The aerodynamic force and hydrodynamic inertia of the payload are negligible.
- There are five degrees of freedom, with the roll of the parachute about its axis of symmetry being ignored.
- The hydrodynamic mass and moment of inertia tensors of the canopy are approximated by single scalars.

- The aerodynamic forces are assumed quasi-static and based on the instantaneous canopy angle of attack.
- The canopy center of pressure is taken at the canopy centroid.
- A flat earth is assumed with no winds.

Translational

$$\frac{dU}{dt} = \frac{X - m_{sys} g \sin\theta}{m_{tot}} - QW$$

$$\frac{dV}{dt} = \frac{Y + m_{sys} g \cos\theta \sin\varphi}{m_{tot}} + PW$$

$$\frac{dW}{dt} = \frac{Z + m_{sys} g \cos\theta \cos\varphi}{m_{tot}} - PV + QU$$

Rotational

$$\frac{dP}{dt} = \frac{M - m_p g L_p \cos\theta \sin\varphi + m_c g L_c \cos\theta \sin\varphi}{I_{tot}}$$

$$\frac{dQ}{dt} = \frac{N + \sin\theta \left(m_p g L_p - m_c g L_c\right)}{I_{tot}}$$

Euler Angles

$$\frac{d\theta}{dt} = Q \cos\varphi$$

$$\frac{d\varphi}{dt} = P + Q \sin\varphi \tan\theta$$

$$\frac{d\psi}{dt} = Q \sin\varphi \sec\theta$$

Other

$$m_{app} = \pi K_{app} \rho {D_o}^3$$

B. System Overview

The parachute aerodynamics used in this study is based from that of a Viking style Disk-Gap-Band. The parachute dimensions and mass properties are for a large 33.5m nominal diameter canopy, as defined in Table 1. Unless mentioned otherwise, the following parameters are held constant in each of the sensitivity studies presented in this paper. Further, since the vehicle is assumed to be a point mass, its only applicable properties include a mass & mass moment of inertia of 1,300 kg & 1,600 kg·m^2.

Table 1. Canopy Design Characteristics

Type	Disk-Gap-Band
Mass	150 kg
Diameter	33.5 m
Trailing Distance	60 m
Moment of Inertia	10,500 kg·m^2
Apparent Mass Coeff. (K_{app})	0.035

C. Simulation Setup

Unless otherwise specified, the following conditions in Table 2 are used throughout this analysis. Although the initial velocity is much slower than should be expected in a re-entry scenario, it is loosely representative of that from a low-velocity airdrop test. This causes inherent flaws with using the upper-altitude in these sensitivities since the system is not at a steady state descent. For this reason alone, data above 40km will not be referenced in making most of the conclusions from this study, but the simulation will always be initialized as described below.

Table 2. Additional sim setup details

Atmosphere	1976 Standard, No wind
Initial Velocity	[0 0 100] m/s
Initial Altitude	80km AGL

III. Parachute System Instability Modes

In an effort to gain further understanding of different parachute instability modes, the system of equations are used as a vehicle to explore various potential causes of instability. Sources that have been addressed include initial condition state of the system, wind disturbances, and various altitude ranges. Due to lack of aerodynamic data for an Earth entry parachute system, a system configuration similar to that of a notional drop test will be used in an Earth standard atmosphere.

A. Pitch Instability

The first instability mode may seem somewhat uninteresting at first since it effectively limits the system dynamics to a single plane. However, it is certainly valuable to build an understanding of how the system will behave starting from this simpler example. Additionally, the progression and regression of stability through the altitude range is an early indication of the main theme of this paper.

1. Initial Conditions Characterization

As could be expected, the system shows a very similar response to non-zero pitch angles and pitch rates. Even for various ranges of non-zero initial pitch angles combined with rates have similar results.

The first case considered starts with a 10˚ initial pitch angle. Looking at Figure 1, the trajectory begins to converge to a single isobar (~6kPa). In Figure 2, the system is dampening in the high-altitude phase of descent—reaching stable flight around 45 km, which also aligns well with the altitude range where the canopy added mass becomes more significant in Figure 4. Notice that all of these effects occur as the system approaches the steady state dynamic pressure.

Figure 3 zooms closer into the unstable low altitude phase of flight. In this figure a small offset of 10˚ is still applied to the initial pitch angle and has small residual dynamics in the mid altitude phase of descent. As the system reaches altitudes less than 8 km above ground level (AGL), the added mass of the canopy becomes large enough such that the system center of gravity (CG) is getting closer to the canopy center of pressure (CP), thus reducing its control authority to dampen these residual angular rates still remaining. A sensitivity exploring the effects of the CG location on system stability is covered more thoroughly later in this paper.

When the same plot using a large initial pitch angle offset of 70˚ is compared to that of the small offset, the dynamics align within tenths of a degree of one another since the damped mid-altitude phase of descent causes these two cases to converge. It can be found that a small & large initial pitch angle offset applied at a high altitude will result in nearly identical instability modes. Different magnitude disturbances at the low altitude portion of flight will be explored through wind gusts later in this paper.

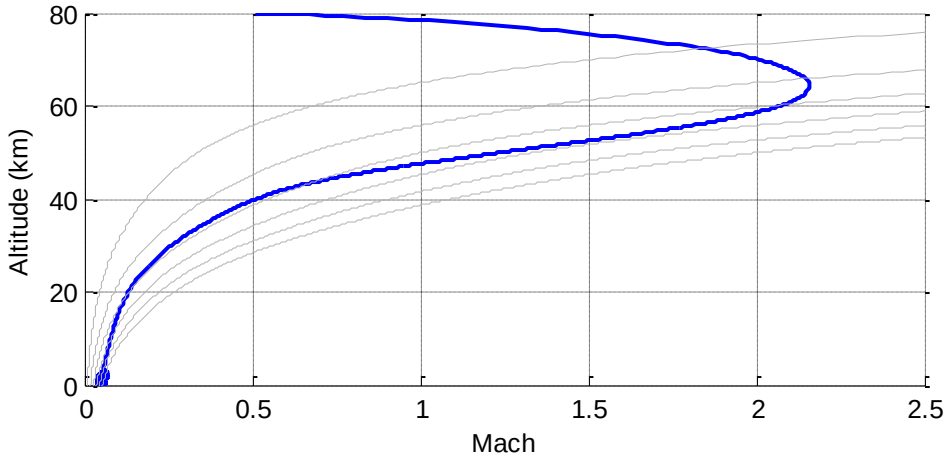

Figure 1. Mach vs. Altitude with dynamic pressure isobars at 2:2:12 kPa

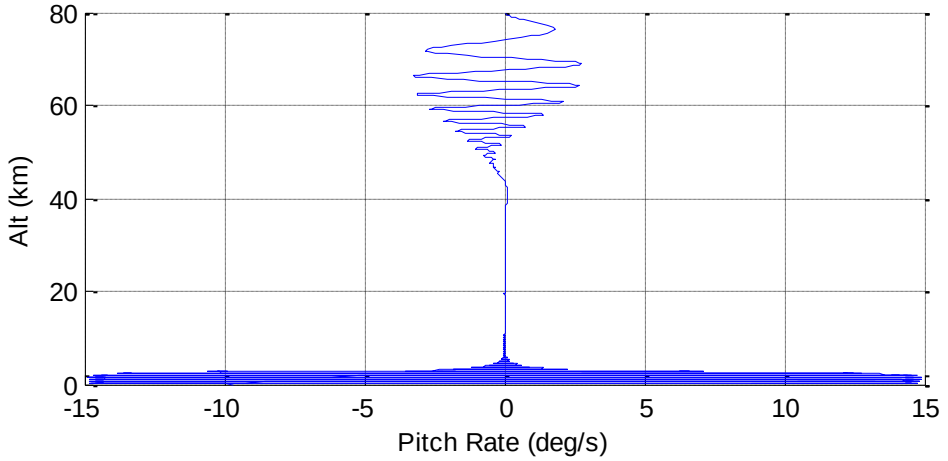

Figure 2. Pitch dynamics dampen and settle near zero at ~45km. This settling is the system reaches a steady state as shown in the previous figure.

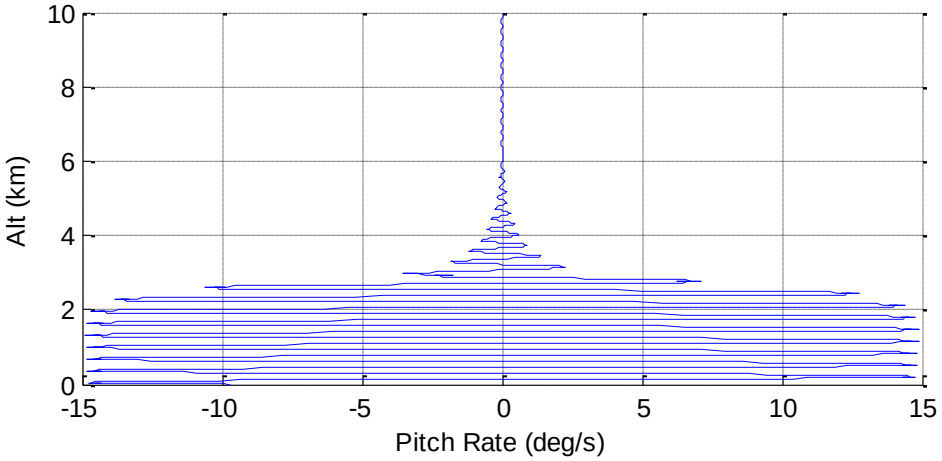

Figure 3. Same as previous figure, but zoomed-in on the unstable low-altitude phase of descent.

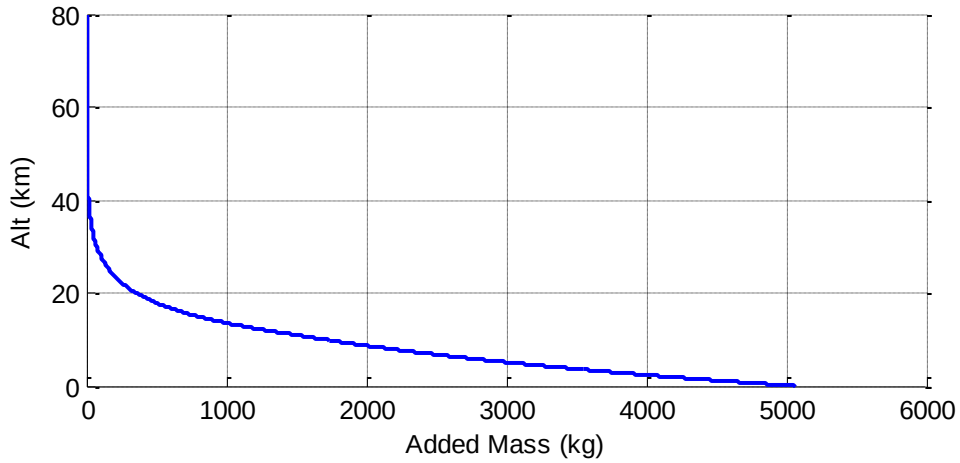

Figure 4. Added mass increases sharply below 40km altitude, aligning with the damped epoch of the mid-altitude portion of descent.

Notice how the significant initial pitch angle of 70˚ can influence the system in a similar manner. Though the larger offset results in larger dynamics in the high altitude phase, this evidence supports the conclusion that the small & large offset cases converge to similar residual rates for the mid altitude phase of descent.

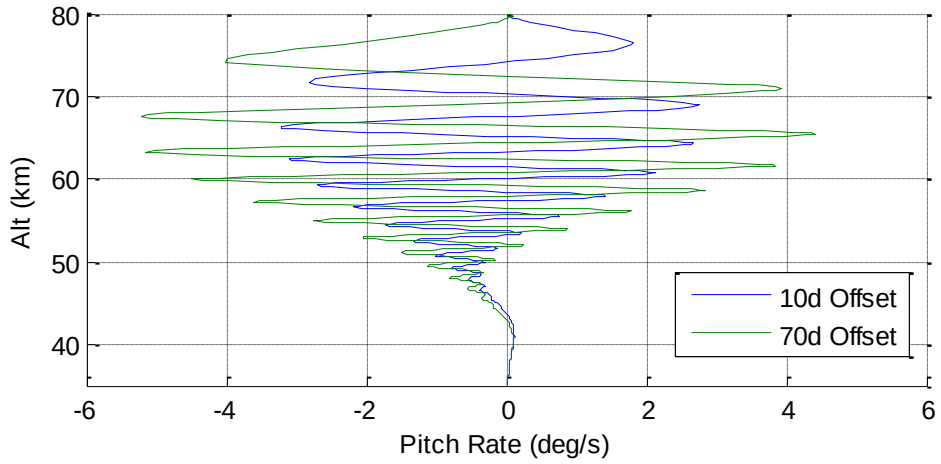

Figure 5. Large intital disturbance on the pitch plane results in similar behavior to that of a small disturbance. Again, damping at ~45km

B. Coning Instability

As will be shown, coning motion of a parachute system can be expected when non-zero initial conditions are mixed between different planes of motion. Similar to that of the Large Angle Pitching section, non-zero initial pitch rate and combined pitch angle & rate will not be covered due to their characteristically similar behavior.

Before observing results from a small non-zero initial pitch & yaw angle of 1˚, it is important to note that the initial dampening of the system in the high altitude phase of descent behaves similar to that shown in the pure pitch instability examples. In Figure 6, the coupled rates seem to damp out and stabilize when reaching the 40-45km altitude range. Since it can be confusing to show both the pitch & yaw angular rates concurrently on the same figure, the root sum square (RSS) of these two rates is provided instead.

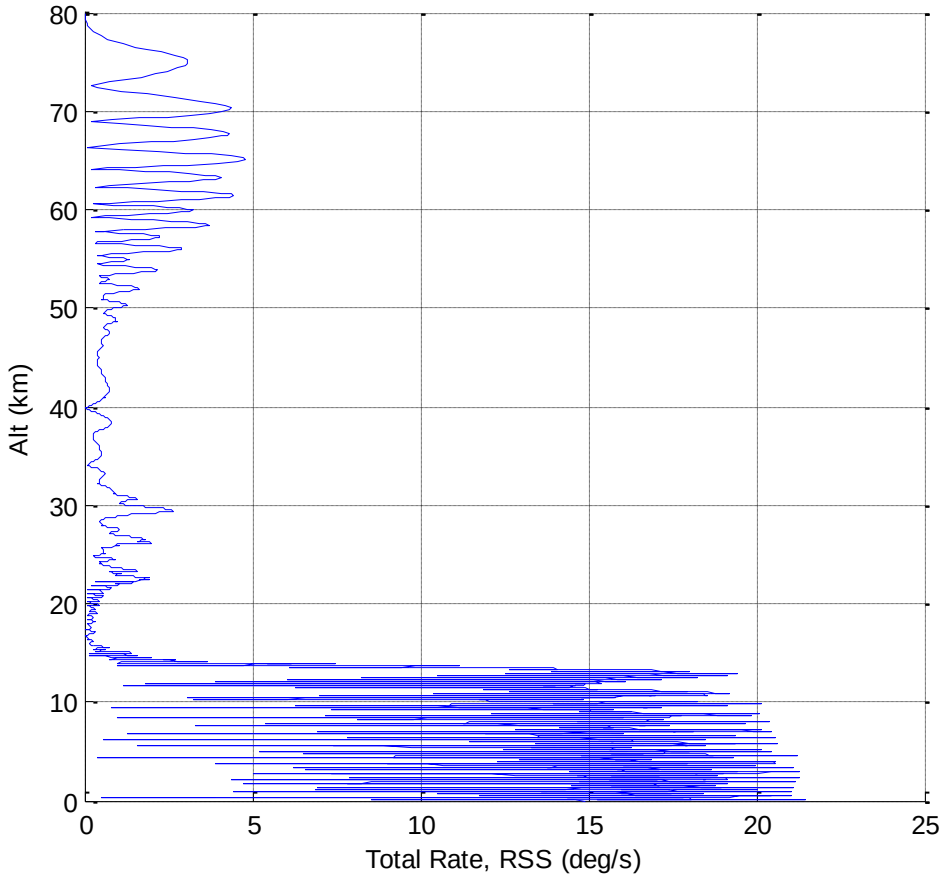

Figure 6. Coupled pitch/yaw dynamics damp intitially and begin an unorganized coning motion in low-altitude flight.

Of particular interest when looking for coning motion is a coupling of rates between the pitch & yaw planes. Since angular rates about both axes are shown as a RSS in Figure 6, the coupling effect is best represented when the two planes of motion are concurrently shown as is in Figure 7. Take note that the rates above 40km do not couple in a manner that is indicative of coning, rather they are coupled in a manner that is similar to pure pitch dynamics—only crossing between the pitch/yaw planes.

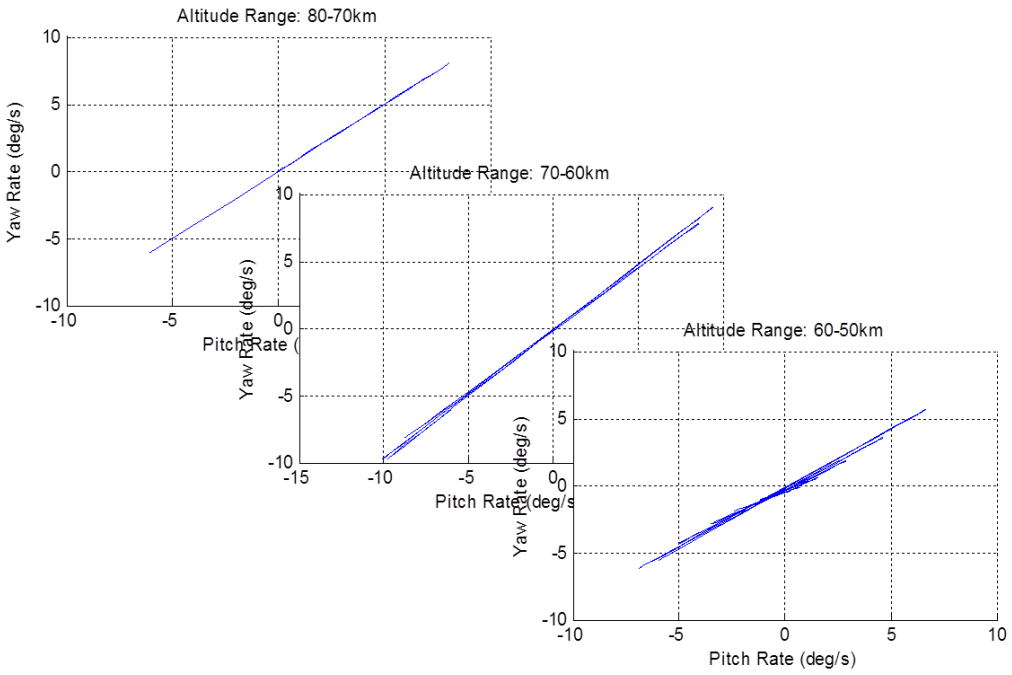

Figure 7. Nearly planar motion in high altitude flight.

Until the system enters a region of flight within which the added mass effects become quite significant, it does not demonstrate any coning behavior, such as that shown in Figure 8. Though this coning behavior is not a very "textbook" example, it is a good indication of how the dynamics across both planes of motion can couple and make it difficult for the total rotational energy to cease. Since this instability mode was not demonstrated until the lower altitude phase of descent, it can be concluded that the CG location relative to the canopy CP is a significant factor that can lead to coning instability—similar to that shown in the pure pitch example. As the canopy added mass increases, the CG location moves increasingly closer to the canopy CP. As the system descends below 40km AGL, the added mass becomes significant enough to move the CG slightly, but consistently, towards the canopy, shown in Figure 9.

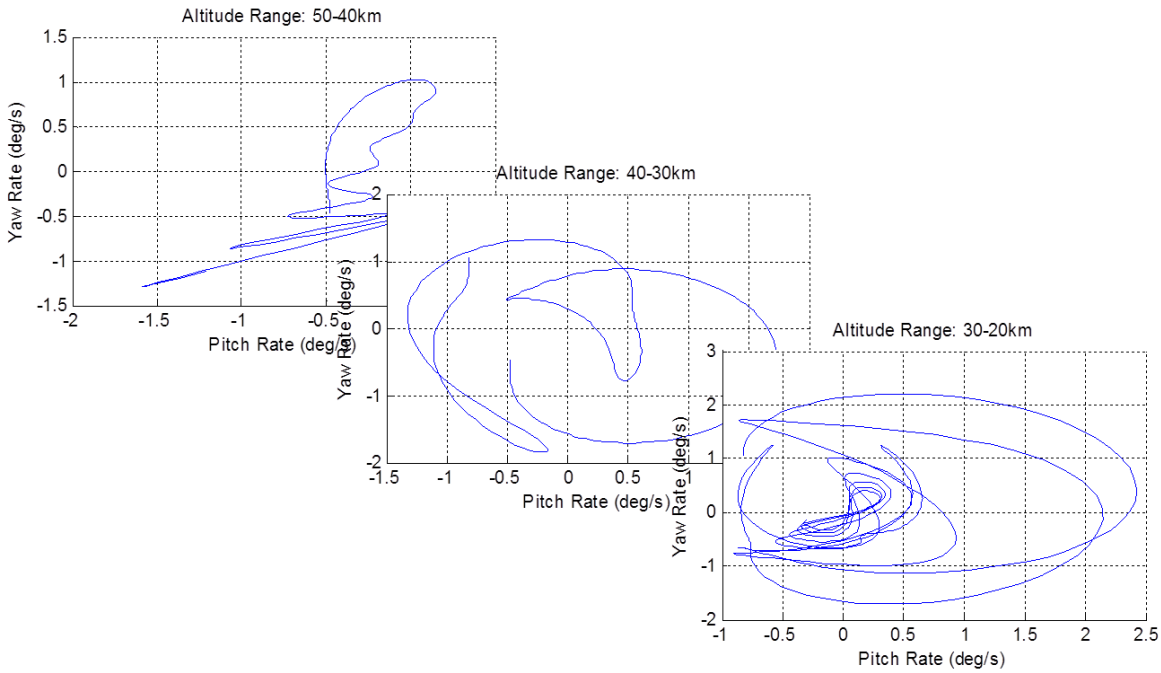

Figure 8. Re-excited into a light coning motion as it descends deeper into the atmosphere.

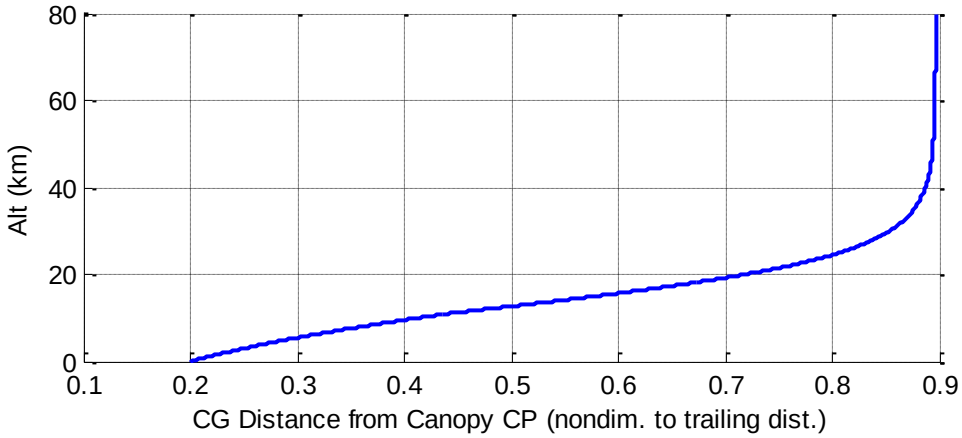

Figure 9. CG Distance from the canopy CP, normalized by the canopy trailing distance.

Before touchdown, the system coning motion becomes more significant with a moving RSS axis of rotation. With a static RSS axis of rotation, these coupled plots would look more like a circle or ellipse.

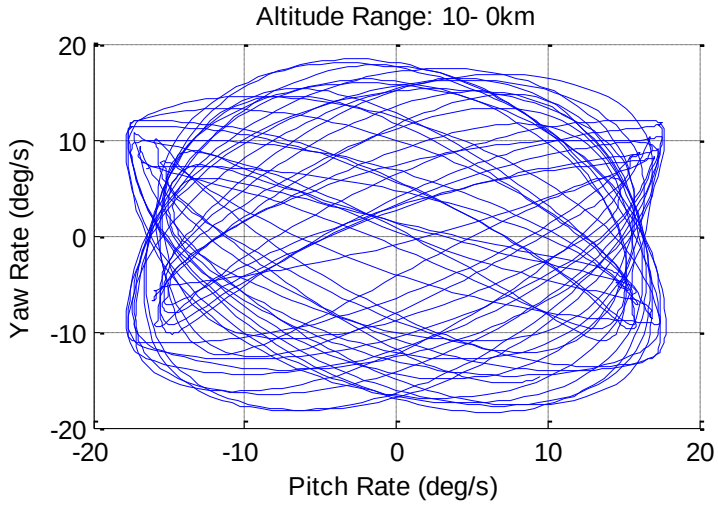

Figure 10. Final region of flight is very dynamic and shows evidence of coning.

Moving to a larger offset at the initial pitch & yaw angles, an offset of 20˚ is considered for this case. As can be seen in Figure 11, the upper altitude rotational energy is again limited to a single plane with coupled motion between pitch & yaw. However, a key difference with the larger initial condition offsets is the characteristic and consistent pure coning motion observed from 50 km through 20 km. Since the larger offset angles result in a larger residual rotational energy across the pitch and yaw planes, the coning motion begins at a higher altitude than the previous example. By allowing more altitude for the system to progress into a more organized coning motion, the simulation results in a more representative example of coning instability, as shown in Figure 12.

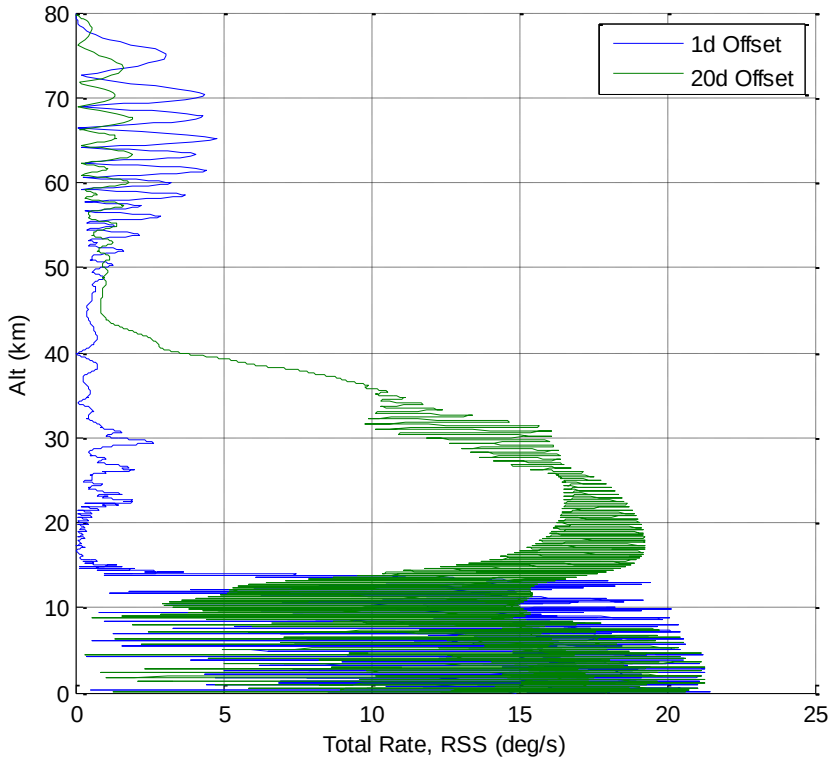

Figure 11. Large, coupled initial disturbance results in similar coupling characteristics throughout the trajectory, but more significant.

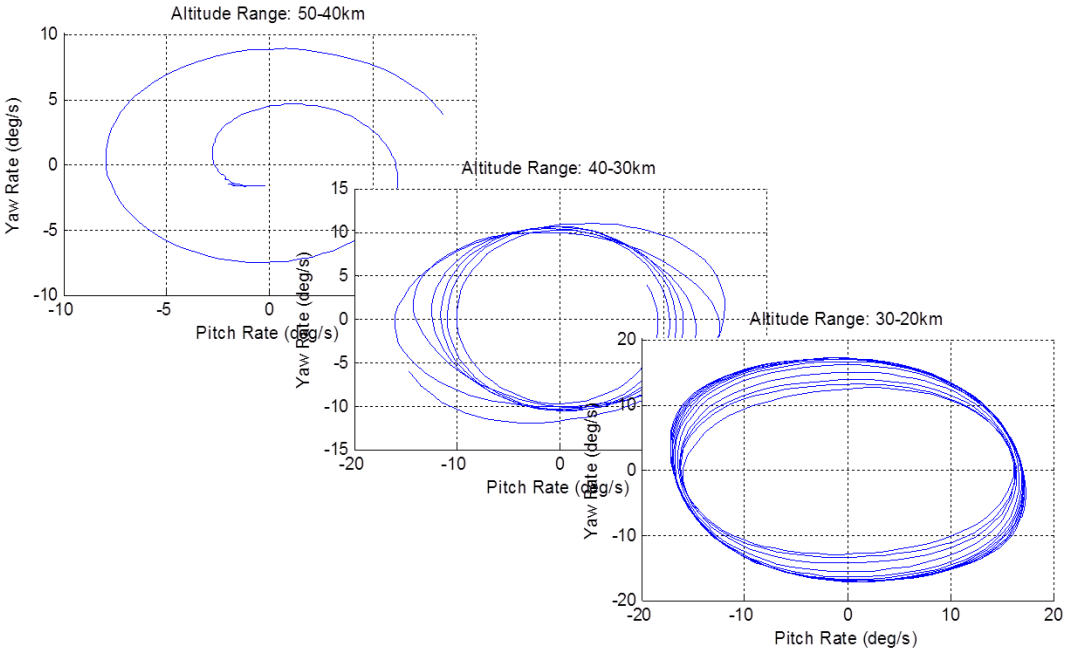

Figure 12. Definitive coning motion is initiated around 40km altitude and becomes more organized within 10km

Interestingly enough, as the system is falling through the final 10km, the dynamics begin to re-align with that from the small initial condition offset example. This is likely due to the added mass completely dominating the system motion and the initial conditions from 70 km above have been washed out to a very high-order effect on the trajectory.

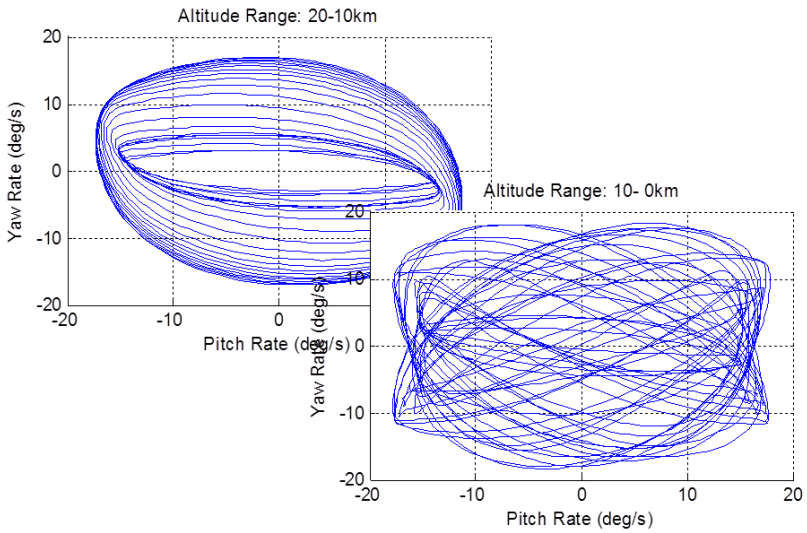

Figure 13. The final 20 km of flight begins to converge into similar behavior shown from the small disturbance example.

C. Wind Disturbance Effects

By incorporating wind gusts into the same model, one can gain an understanding of how the system can recover from such an uncontrollable factor. This sensitivity considers small (1 m/s) and large (25 m/s) wind gusts in two different manners: 1) along a single axis (pitching), and 2) combined across two axes (coning).

First, considering small & large wind gusts along a single axis at 20 km altitude, the system aerodynamics provide enough control to initially damp the system quickly; however, due to the small residual pitch motion that remains, the system becomes unstable below 10 km due to the reduced control authority of the canopy aerodynamics. This behavior was nearly identical for both large and small gusts along a single axis.

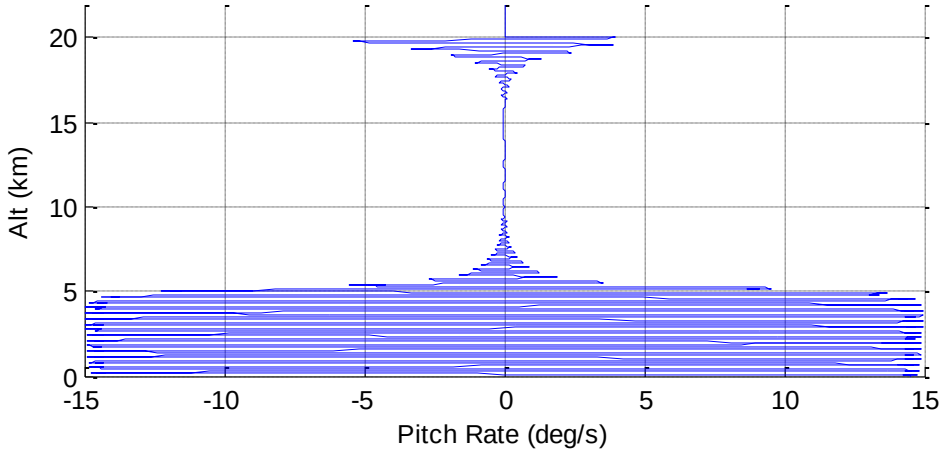

Figure 14. Small & large wind disturbances along a certain axis result similar highly damped response from the system. The small gust example is shown here.

For wind gusts that are directed across two axes, it can be expected to impart a moment on the system that can result in a coning instability mode. This expectation is proved to be accurate in Figure 15 & 16. Referring back to the single axis wind gust example, the system reacts to the cross-axes wind gust more quickly and results in a very prominent coning instability mode. Since the behavior is again observed to be nearly identical with small & large wind gusts, it can be concluded that the gust behaves as the catalyst to instability & the system design sustains the instability.

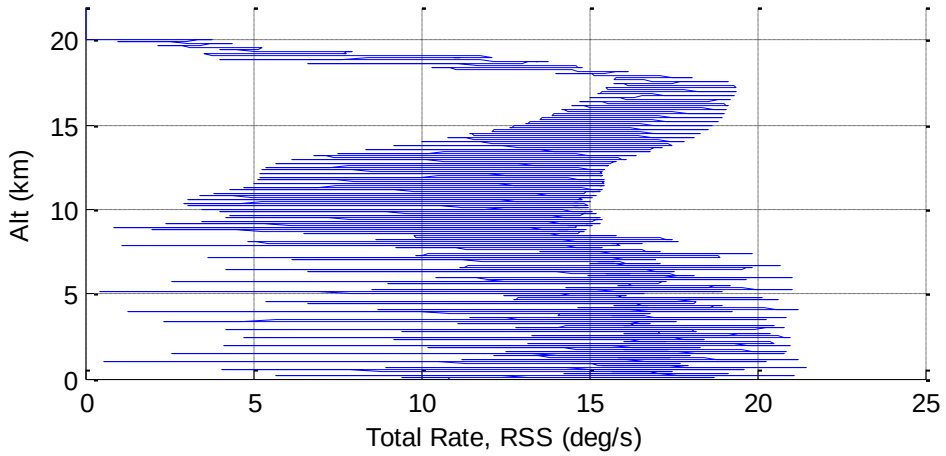

Figure 15. Unlike the single axis wind gust, a gust coupled across planes immediately perturbs the system into a significant coning instability mode.

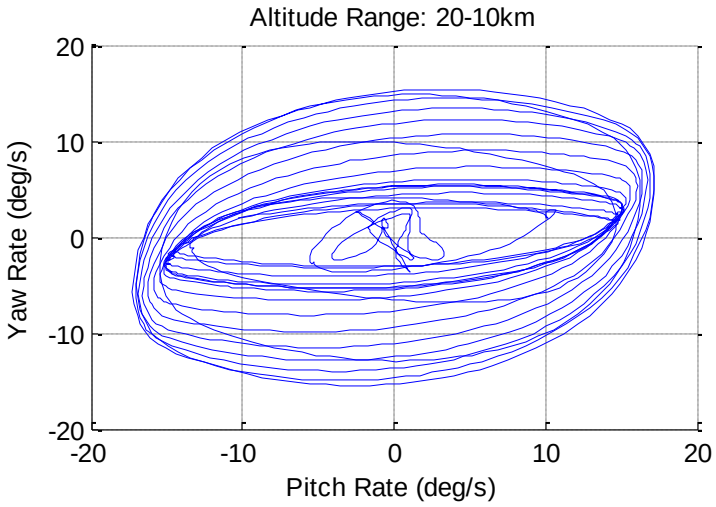

Figure 16. Coning motion becomes evident soon after the coupled wind gust at 20km.

D. System Characterization

To further understand these modes of instability, it is beneficial to explore how the system design can influence these instability modes. A few sensitivity studies are explored next and are approached with the pitching instability mode in mind to assist in generalizing solutions.

As has been proven through the legacy of parachute design & testing, as the canopy trailing distance increases for a particular system and application, its stability will improve. This is largely due to the increased moment arm length of the parachute forces on the system CG. The effect that this system design factor has on this instability analysis further substantiates this fact, as shown in Figure 17. Although the benefit from extending this trailing distance is consistent beyond the baseline configuration, several other design factors must be considered that limit the trailing distance, such as deployment system design, mass growth, inflation characteristics, and previous experience to name a few. The following figure depicts each trailing distance case relative to the nominal canopy diameter.

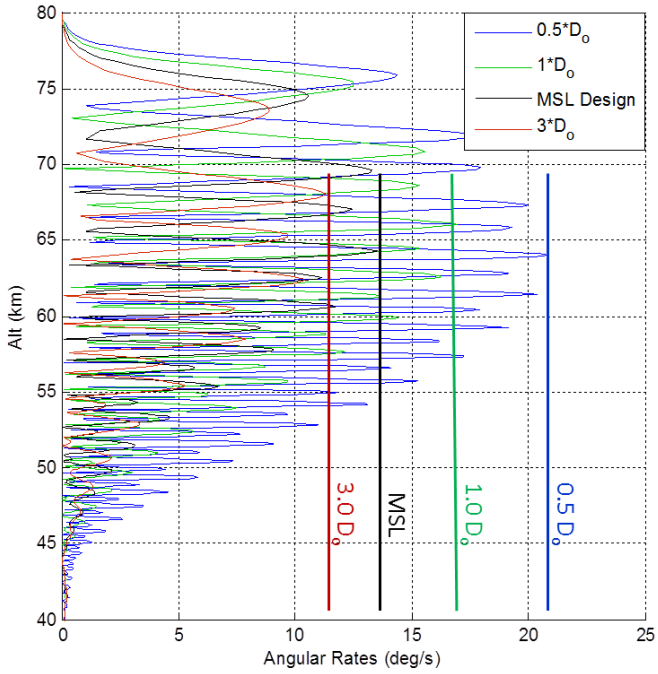

Figure 17. As the canopy trailing distance increases, so does system stability. However, other system design factors limit this distance from being too large.

Considering the canopy diameter, a range will be explored assuming the same initial conditions for each case. Since the airspeed is kept constant, it is apparent that this initial velocity is too slow for the smaller canopies as there is a larger offset to settle into a steady state dynamic pressure as shown in Figure 18. This clearly proves to affect the rotational dynamics as this figure is compared to that shown in Figure 19. Additionally, the mass of the canopy increases by the diameter cubed. As will be described in further detail within the case study, when the total mass (added + actual canopy mass) increases, the imparted moment due to canopy side forces will decrease—resulting in a more stable system.

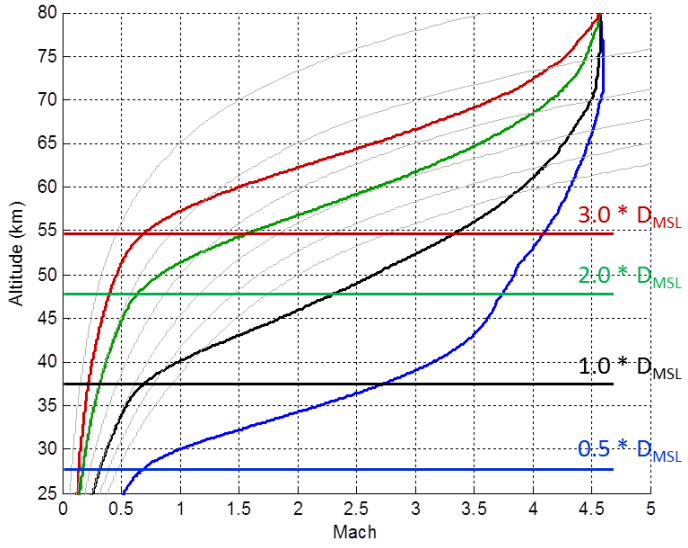

Figure 18. Altitude of steady state dynamic pressure correlates well with the altitude of zero rates.

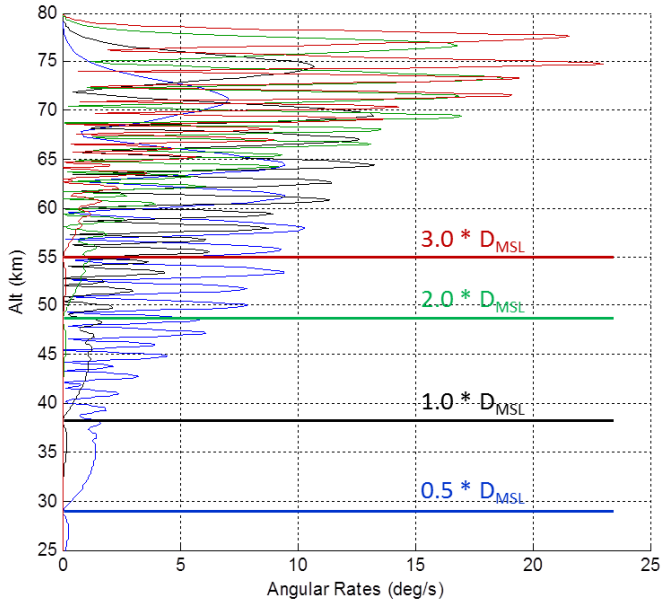

Figure 19. The initial conditions used are not conducive of a smaller canopy.

To address the instability in the lower altitude range of flight, a trade study across a range of payload masses is performed. By relating the altitude of this instability (Figure 20) to the CG location trend (Figure 21) as the system descends to lower atmosphere (i.e. higher freestream density), it is shown that the payload mass has a 1st order effect on when this instability will occur. More specifically, as the CG encroaches within 25-30% trailing distance away

from the canopy CP, system instability quickly diverges. Though this sensitivity is not shown for coning motion, a similar trend can be expected for this stability mode as well.

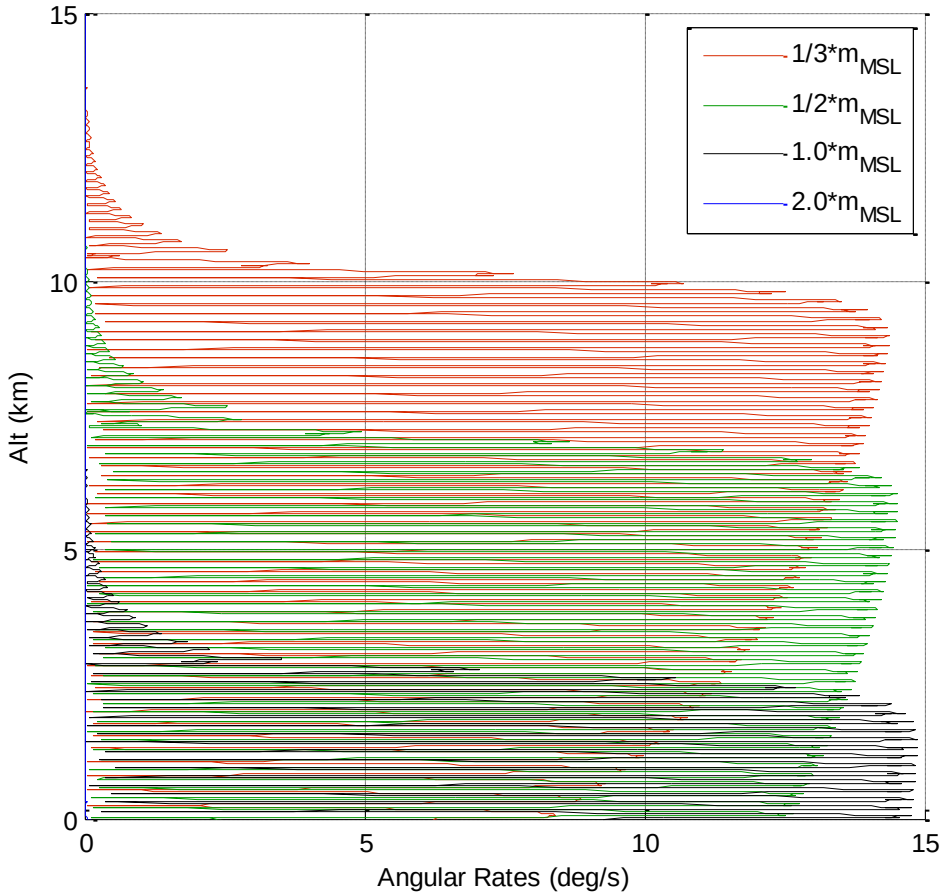

Figure 20. As the payload mass is decreased the system becomes unstable at a higher altitude as the canopy control authority is reduced.

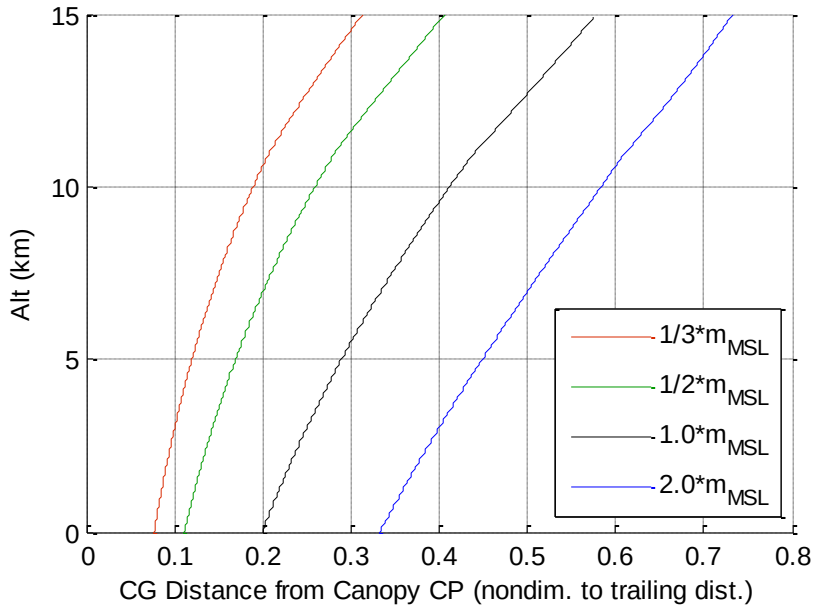

Figure 21. For this system, instability becomes more apparent once the CG is within 25-30% distance to the canopy

IV. Mars Research Drop Test Case Study

In an early phase of Mars EDL research, a Ringsail parachute and Drop Test Vehicle (DTV) system was released from a balloon at high altitude. Shortly after extraction the system began to experience total angle of attack (α_{tot}) oscillations about the system center of gravity (CG). The peak α_{tot} quickly increased and plateaued between 40° and 45° from approximately 70,000 to 57,000 feet altitude. At 57,000 feet the pitching motion abruptly reduced to approximately 20° within a few seconds. Initially, it was theorized that a sharp wind shear recorded just below 60,000 feet imparted enough "counter" energy into the system such that the pitching dynamics damped to a level that was in-family with predictions. Though this wind was certainly a contributing factor, there are other underlying flight & system characteristics that are constructed in this paper to gain a better understanding of why this happened and when it could be expected for other systems. Ultimately, this analysis will show that the vortex shedding resonance behavior is an effect of testing a canopy in an environment for which it was not intended—this anomaly was not expected in a "typical" Mars descent environment (i.e. atmosphere & trajectory).

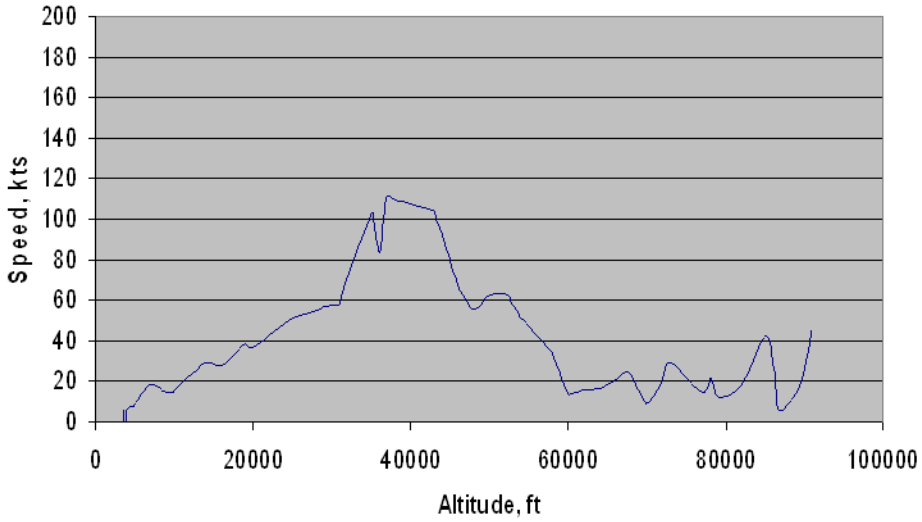

Figure 22. Upper wind profile from the high-altitude drop test

A. Theory Overview

As mentioned, the physical cause of this behavior is primarily due to the parachute vortex shedding (PVS) frequency resonating with that of the integrated system (parachute and payload) natural frequency. At high altitudes, the freestream density is sufficiently low to result in a relatively small ratio of apparent mass to payload mass—causing the system CG to be located at a point very close to the payload. This results a long moment arm between the canopy and the system CG such that the PVS behavior can dominate the system dynamics. As illustrated in Figure 3, the moment imparted by the force resulting from the PVS (depicted by F_{PVS}) can certainly control the motion of the integrated system. If the PVS frequency encroaches on the system natural frequency, as occurred in this drop test, the pitching motion will grow exponentially until it reaches a sort of limit cycle—40˚ to 45˚ in this case. Though this is a challenge for this flight environment, it will be shown that the trajectory design & atmosphere of which typical Mars-entry vehicles fly does not show any risk of similar resonance. The considered Ringsail canopy in low altitude descent is less prone to this behavior since the parachute added mass becomes large enough to result in a smaller F_{PVS} moment arm (depicted by L_{CG} in Figure 3).

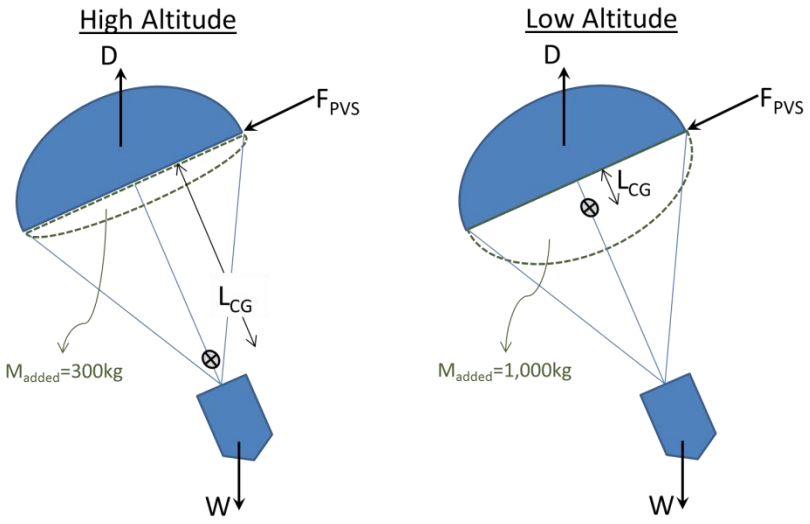

Figure 23. Added mass has a significant effect on the excitation side force resulting from the PVS-induced motion.

B. Analysis and Equations Used

In determining the validity of this theory, a sequence of calculations can be derived with various simplifying assumptions to determine the approximate natural frequency of the system. This can then be compared to that of the PVS frequency (based largely from an assumed Strouhal number) to prove that the oscillations was likley due to PVS resonance.

Initially, to approximate a velocity profile, it is assumed that the parachute system is at a vertical, steady-state descent.

$$V_{term} = \sqrt{\frac{(m_{chute} + m_{dtv})g}{0.5\rho(C_d A|_{chute} + C_d A|_{dtv})}}$$

where ρ is the freestream density. Apparent mass is approximated with the following relationship,

$$m_A = C_{HS}\rho\frac{2}{3}\pi\left(\frac{d_p}{2}\right)^3$$

where C_{HS} represents the half-sphere coefficient (assumed to be 2.5 for this application) and d_p is the parachute projected diameter.

In characterizing the rotational dynamics of the system, the canopy moment of inertia is approximated through the following relationships.

$$I_{chute} = \frac{2}{3}m_{chute}(C_d\frac{d_0}{2})^2$$

This is then translated to the system CG with the following sequence of equations…

$$d_{dtv2cg} = d_{chute2dtv}\frac{m_{chute} + m_A}{m_{chute} + m_{dtv} + m_A}$$

$$d_{chute2cg} = d_{chute2dtv} - d_{dtv2cg}$$

$$I_{chute,CG} = (m_{chute} + m_A){d_{chute2cg}}^2 + I_{chute}$$

where d_0 is the parachute nominal diameter and $d_{chute2cg}$ is the distance from the canopy center of mass to the system center of mass. Further, the drag of both system elements is estimated through traditional means.

$$D_{chute} = qC_{d_{chute}}\pi\left(\frac{d_0}{2}\right)^2$$

$$D_{dtv} = qC_{d_{dtv}}A_{dtv}$$

where q represents the dynamic pressure. Finally, sufficient system parameters are known to determine a reasonable approximation of the system natural frequency.

$$\boldsymbol{f_n = \frac{1}{2\pi}\sqrt{\frac{d_{dtv2cg}(m_{dtv}g - D_{dtv}) + d_{chute2cg}(D_{chute} - m_{chute}g)}{I_{sys}}}}$$

Fortunately, by estimating the canopy Strouhal number, a non-dimensional parameter that is used in describing oscillating flow mechanisms, the Strouhal number equation can be rearranged to solve for PVS frequency.

$$\boldsymbol{f_{PVS} = \frac{S_t V_{term}}{d_{ratio} d_0}}$$

where S_t corresponds to the canopy Strouhal number. The canopy Strouhal number is estimated to be 0.17, based on C.Q. Shen's and D. J. Cockrell's paper [2]. Due to the obvious dependency that the PVS frequency has on the Stouhal number—a very sensitive & complex value to measure or estimate—this factor will be further explored as a trade space later in the paper.

C. Results and Where Resonance Occurs

By comparing the results obtained through this series of calculations to the drop test data, the PVS resonance theory can be further substantiated. As shown in Figure 4, the PVS frequency (f_{PVS}) is approximately equal to the natural frequency of the entire system (f_n) as the vehicle approaches an altitude of ~63,000 feet—the center of the altitude band that the pitch motion limit cycle was experienced. Further, the sharp divergence between these two frequency curves below 63,000ft is telling of the system behavior when the pitch motion reduced. Combining this

with the sudden increase in upper-level winds could account for the first-order influences as to why the pitch dynamics suddenly ceased around 57,000ft, as pointed out in Figure 5.

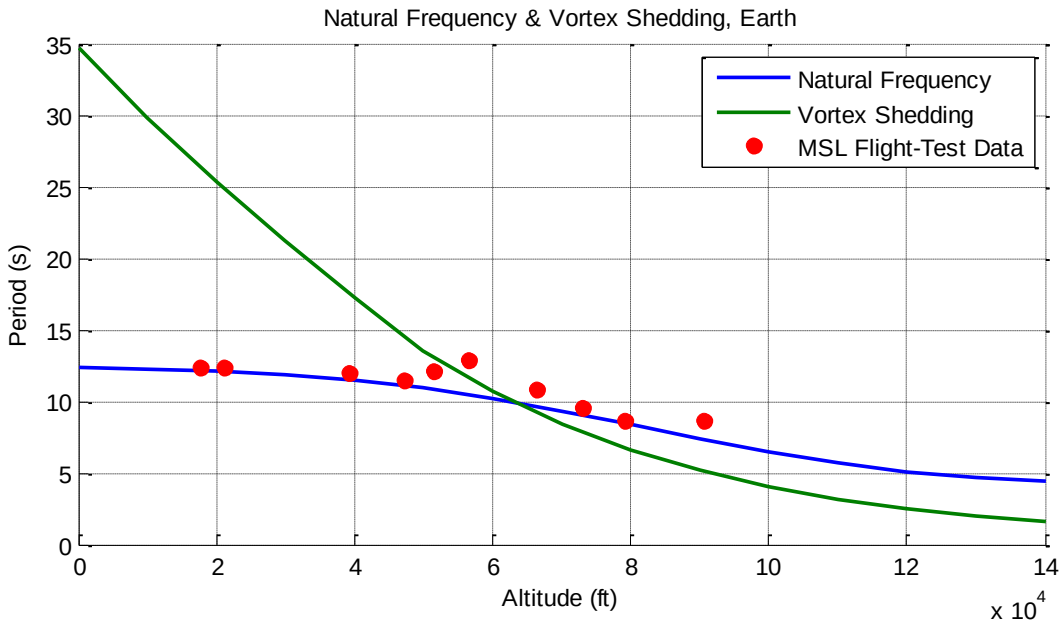

Figure 24. Intersection of the PVS & natural frequency curves provides further evidence of this under-damped pitching motion.

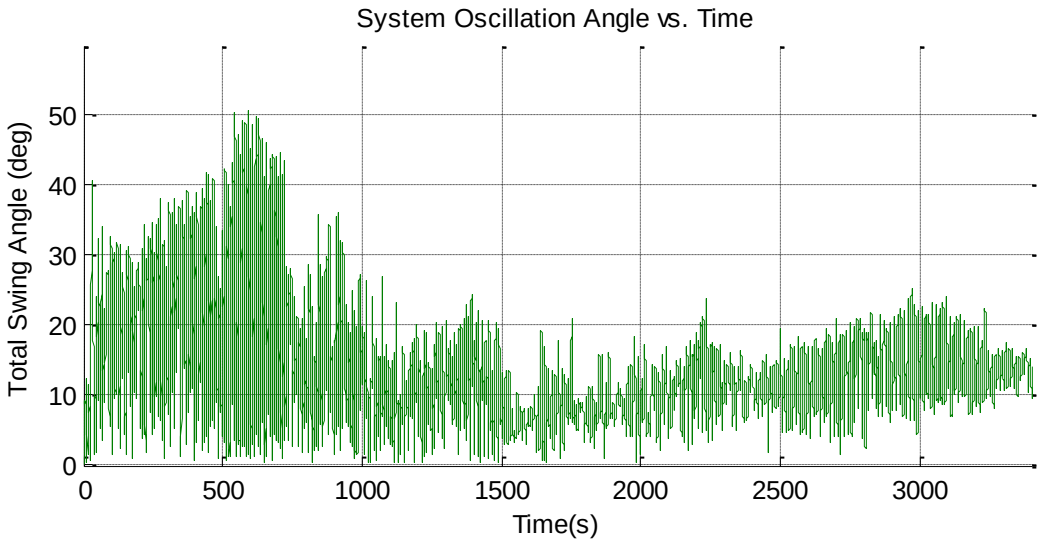

Figure 25. Swing dynamics sharply increase as the Figure 18 curves converge. This motion ceases as the curves cross and quickly diverge.

With these relationships identified, it is useful to determine whether this behavior would be of concern during a more representative Mars-mission descent trajectory. By applying the same theory to the predicted flight system

and environment, the f_{PVS} and f_n is approximated and shown to not intersect or converge in Figure 6. Thus, it is predicted that PVS resonance was not expected during MSL's descent flight phase.

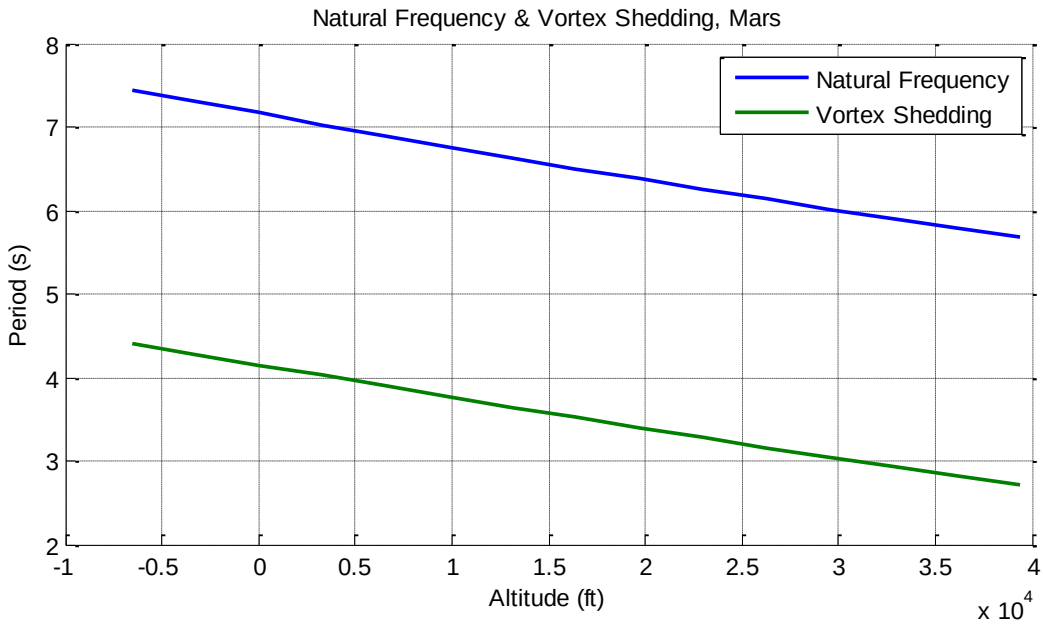

Figure 26. Applying this theory with the same system in a Martian atmosphere shows that this behavior should not be expected.

D. Further Assessment of the Drop Test Case Study

Given the approximate nature of Strouhal number, upper atmospheric winds, system mass properties, canopy added mass, and several other factors that affect the PVS and natural frequency calculations, it would be useful to capture the range of descent within which the system was resonating. By looking at the percent difference between the PVS and natural frequencies along an altitude-velocity profile, one can determine the region of flight within which the PVS frequency resonance began to override the system. By overlaying the MSL drop test trajectory in Figure 7 and referring back to the Figure 5 it can be deduced that the PVS frequency resonance began to control the system when the percent difference reached approximately 20%.

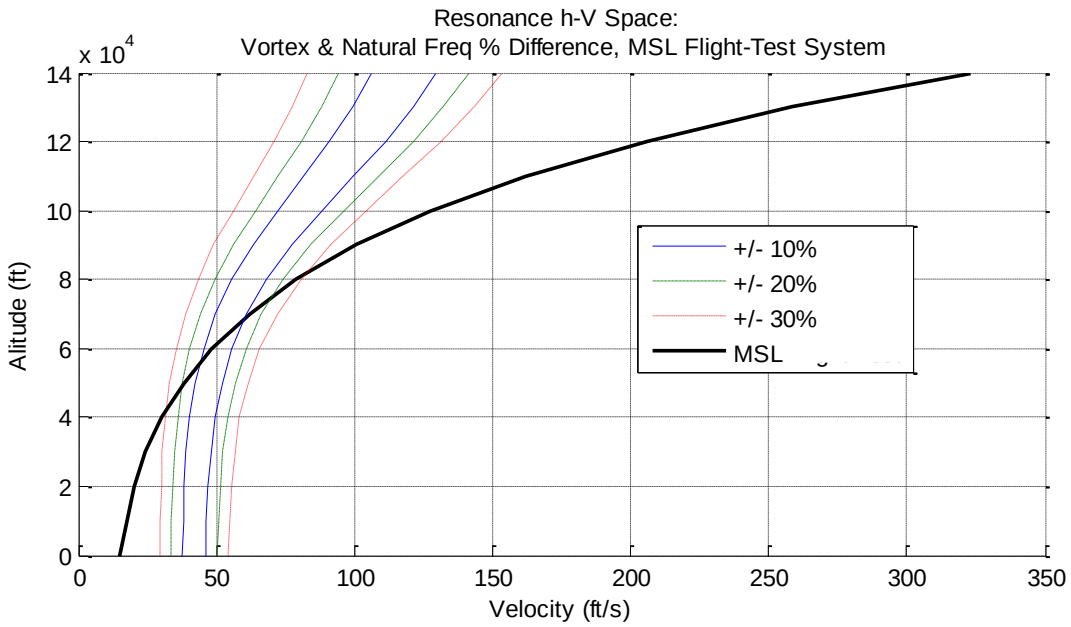

Figure 27. The altitude range of the swing dynamics aligns well with that of a +/-20% difference in PVS & system natural freqency

E. Bounding the Problem

In this work, the previous equations & theory could be applied towards mission design by determining a set of system type and flight environment bounds, within which the system is in risk of experiencing similar swing oscillations due to PVS resonance. This proposed method of bounding PVS resonance assumes fixed physical dimensions and mass properties of the canopy and vehicle for each set of results. Due to its indefinite nature during flight and the difficulty in measuring it, the canopy Strouhal number is used as the sole "degree of freedom" to characterize the flight system. This method was established to achieve a robust and unambiguous reference in determining whether further analyses and/or drop tests are necessary to decide whether the risk of PVS resonance is acceptable for whatever application is in question.

To provide additional clarity and flexibility to the designer, two approaches to bounding PVS resonance is provided. In the case that the designer prefers to reference a "critical" Reynolds number, a design space showing a critical Reynolds number contour within an altitude vs Strouhal number space is determined. "Critical" Reynolds number refers to the Reynolds number at which PVS resonance is likely for a certain altitude and Strouhal number combination. Another approach to show this data is with a "critical" Strouhal number contour throughout an

altitude vs velocity space. "Critical" Strouhal number refers to the Strouhal number at which PVS resonance is likely for a certain altitude and velocity combination.

2. "Critical" Reynolds Number

Effectively, this figure allows for the designer to reference the altitude range of interest for their specific canopy design (i.e. Strouhal number). If the in-flight Reynolds number is within +/-30% of the critical Reynolds number for the same altitude and Strouhal number, it can be concluded that further assessment and/or design refinement is necessary to fully understand the risk of PVS resonance. The 30% refers to the range of flight conditions within which the drop-test began and continued to experience increasing amplitude oscillations.

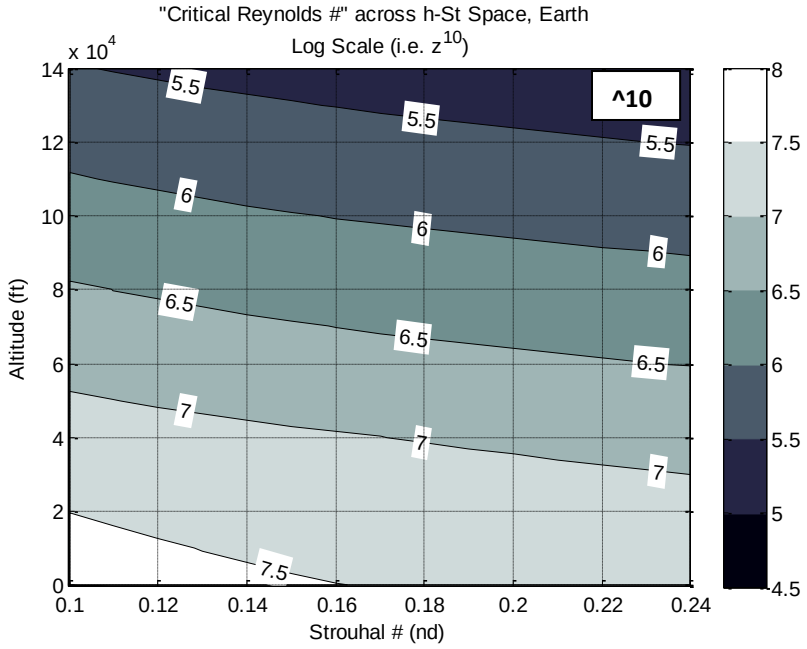

Figure 28. A critical Reynolds number could be referenced to predict this behavior. Earth atmosphere

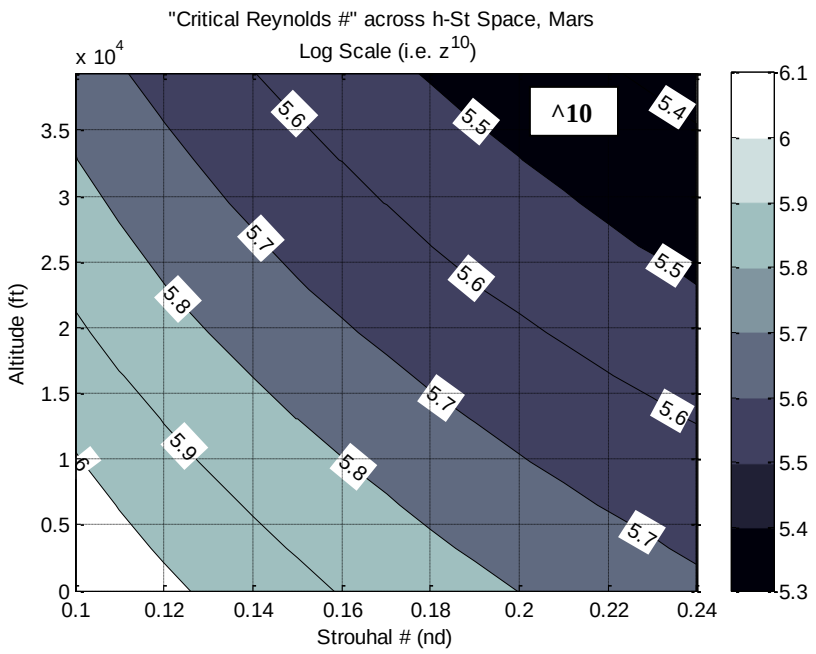

Figure 29. A critical Reynolds number could be referenced to predict this behavior. Martian atmosphere

Unfortunately, the altitude vs. Strouhal number profile is an uncommon profile with mission and flight design and is difficult to use to visualize the vehicle's flight. For this reason, it can be useful for the mission designer to reference the canopy Strouhal number along an altitude vs. velocity profile instead.

3. "Critical" Strouhal Number

By considering a range of likely canopy Strouhal number, the designer can refer to an altitude vs. velocity profile showing the countours of multiple critical Strouhal numbers. If the in-flight Strouhal number is within +/-30% of the critical Strouhal number for the same altitude and velocity, it can be concluded that further assessment and/or design refinement is necessary to fully understand the risk of PVS resonance. The 30% refers to the range of flight conditions within which the MSL drop-test began and continued to experience increasing amplitude oscillations.

The intersection of the 0.17 Critical Strouhal number (red) and the drop-test trajectory (cyan), denotes where the PVS frequency resonated with the system natural frequency. In considering a 30% range of possible Strouhal numbers, the designer must consider Strouhal number values from 0.119 to 0.221—which approximately align with the same altitude range in which large swing angle oscillations occurred in the drop test.

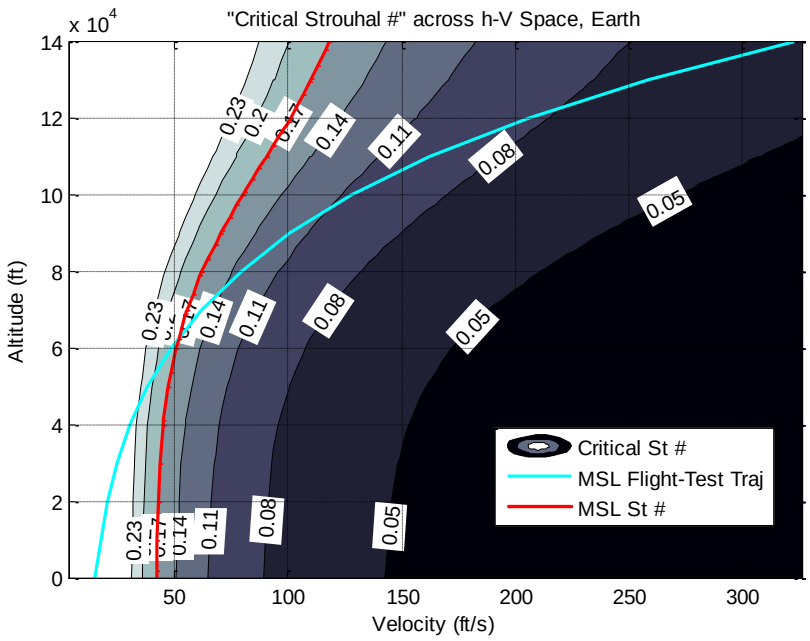

Figure 30. Strouhal numbers of concern for this behavior should not be limited to a single value, but a range.

By applying this tool to the planned MSL flight on Mars, the designer can determine if there is a similar intersection between the in-flight Strouhal number range (0.119 to 0.221) and Critical Strouhal number contours. As shown in Figure 11, this is not the case—providing further evidence that the MSL system is not in considerable risk of experiencing PVS resonance.

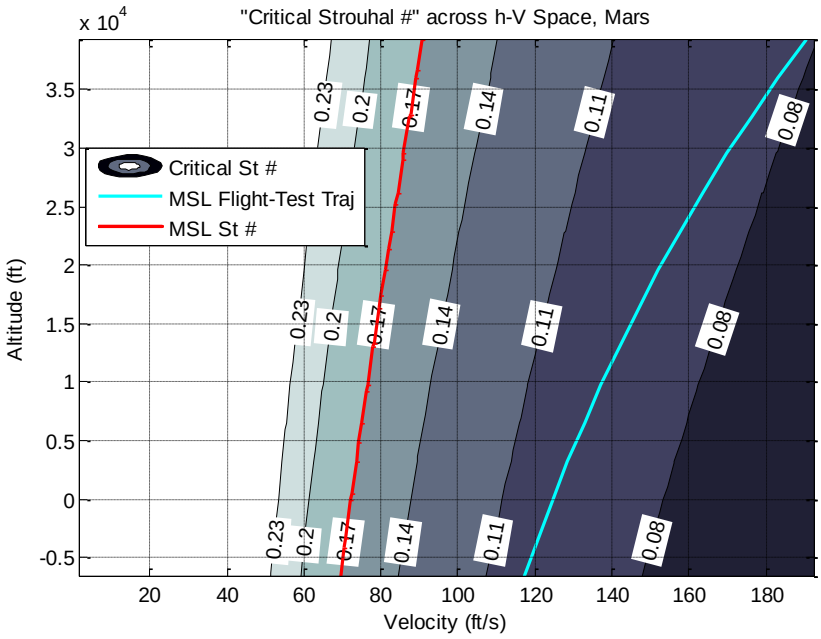

Figure 31. Further evidence that this behavior should not be anticipated for MSL's intended flight envelope.

V. Conclusion

Through the adoption of equations of motion adopted from the White/Wolff paper, pure pitch & coning instability modes have been modeled and characterized using an MSL-like system for Earth entry. By looking at different non-zero initial conditions and combining them in different ways, the most common conclusion across the sensitivities was the potential for high instability when a system is placed in an environment for which it was not designed. Further, the early Mars research subsonic high-altitude drop test case study provided an example of this characteristic and how this has been experienced in the past. This case study also provided an opportunity to bound the environment & system within which the swing oscillations could be expected.

References

[1] White, Frank M.; Wolf, Dean F.. (1968). A Theory of Three-Dimensional Parachute Dynamic Stability. Journal of Aircraft. 5 (1), 86-92.

[2] "Flow Field Characterisation around Cup-Like Bluff Bodies, Parachute Canopies" AIAA 91-0855-CP